International Communications in Heat and Mass Transfer 117 (2020) 104792

Contents lists available at ScienceDirect

International Communications in Heat and Mass Transfer

journal homepage: www.elsevier.com/locate/ichmt

Transient three-dimensional heat conduction in heterogeneous media: Integral transforms and single domain formulation

Anderson P. de Almeida[a,b], Carolina P. Naveira-Cotta[a,*], Renato M. Cotta[a,c]

[a] Laboratory of Nano & Microfluidics and Microsystems – LabMEMS, Mechanical. Eng. Dept., POLI & COPPE/UFRJ, Federal University of Rio de Janeiro, Caixa Postal 68. 503, Rio de Janeiro, RJ 21945-970, Brazil
[b] Petrobras S.A., Rio de Janeiro, Brazil
[c] General Directorate of Nuclear and Technological Development, DGDNTM, Brazilian Navy, Rio de Janeiro, RJ, Brazil

ARTICLE INFO

Keywords:
Heat conduction
Integral transforms
GITT
Heterogeneous media
FGM
Composite medium
IGBT
Electronics cooling
Eigenvalue problem

ABSTRACT

A hybrid numerical-analytical methodology based on integral transforms is employed for solving transient three-dimensional heat conduction problems in heterogeneous media comprising arbitrarily space variable thermophysical properties, including configurations with multiple subdomains of different materials and geometries. The Generalized Integral Transform Technique (GITT) is used to solve for both the temperature distribution and the corresponding eigenvalue problem accounting for the spatially variable coefficients. A previously introduced single domain reformulation strategy is adopted when multiple subdomains are involved, so as to rewrite the heat conduction equation in terms of coefficients with abrupt variations in the spatial coordinates. The hybrid numerical-analytical approach is demonstrated for three classes of problems in which the thermophysical properties undergo significant variations throughout the domain, such as: (i) FGMs (Functionally Graded Materials) with three-dimensional space variable thermophysical properties; (ii) composite medium with inclusions of different geometries and thermophysical properties; (iii) a multi-scale/multi-material heat conduction problem in a IGBT (Insulated Gate Bipolar Transistor) module. In each considered application, both the temperature eigenfunction expansions and the associated eigenvalue problem solutions are critically analyzed in terms of convergence rates and co-verified with purely numerical solutions.

1. Introduction

Naturally occurring or engineered materials are in many cases not homogeneous and thus may present spatially non-uniform physical properties. Even employing cells that are formed of homogeneous materials, structured media can be assembled in ways that result in physical behaviors that are characteristic of the inherent heterogeneities, thus not amenable to homogenization-type approximations. In recent years, with the development of materials processing technologies, various structured material systems have been widely designed and manufactured for improved and/or tailored functions, such as in the cases of composites in general [1], functionally graded materials (FGMs) [2], and metamaterials [3]. Due to their unique physical properties and behaviors, these classes of new materials have been extensively used in extreme environments and unique tasks not attainable by known natural materials, with various applications in aerospace, oil exploration, power generation, subsea, and transportation fields. For instance, functionally graded materials are a new generation of composites, with non-uniform micro- or nano-structures and graded macro-properties (e.g. heat conductivity, specific heat, and density, in heat transfer applications) varying as functions of the spatial coordinates. In addition, various engineering systems are intrinsically heterogeneous and formed of multiple components in direct contact, which may be themselves of different materials and geometries, such as in integrated electronic systems [4].

The main difficulty in modeling heat conduction in heterogeneous media is that thermophysical properties vary across the domain, either abruptly, in the case of actual material transitions, or continuously but steeply, such as in functionally graded materials (FGMs). While classical analytical approaches fail to provide exact solutions to this class of problems in light of the arbitrarily variable equation coefficients, purely numerical methods might also require very refined meshes at materials transitions and interfaces. Different variants of semi-analytical or improved numerical methods have been proposed in the literature for transient or steady heat conduction in heterogeneous media, in different application contexts [5–34]. A few hybrid numerical-analytical approaches attempt to benefit from advantages of both treatments, by carrying along analytical steps up to a certain point, and recurring to numerical methods once the analytical advancement is impeded. Here, special attention is

* Corresponding author.
E-mail address: carolina@mecanica.coppe.ufrj.br (C.P. Naveira-Cotta).

https://doi.org/10.1016/j.icheatmasstransfer.2020.104792

Available online 18 August 2020

given to a fairly general integral transforms solution for heat conduction in heterogeneous media proposed by Naveira-Cotta et al. [12], with the heterogeneities being represented by arbitrarily variable space coefficients, including thermophysical properties and source terms, and applied to typical one-dimensional transient formulations. This analytical approach was then employed in the direct and inverse analysis of a number of heat conduction problems, including the previously mentioned situations of FGMs, composites with abrupt variations of thermophysical properties or randomly distributed two-phase dispersed systems [14–17]. This analytical solution requires the solution of the associated Sturm-Liouville problem with space variable coefficients, when an analytical solution is not readily available. However, through the Generalized Integral Transform Technique (GITT) [35–45], a hybrid numerical-analytical approach can be implemented to both handle a nonlinear problem formulation and transform the differential eigenvalue problem into an algebraic matrix eigenvalue problem. Such developments also stimulated the proposition of a single domain reformulation strategy, originally advanced in the context of conjugated heat transfer problems [46–51]. It consists of rewriting a multiregion problem into a single region with space variable thermophysical properties and source terms, and is particularly convenient for handling heterogeneous media problems with multiple regions and different materials. Also, fairly recently, a convergence acceleration scheme has been developed and applied to eigenvalue problems [52], which allows for the treatment of multiscale space variations, due to either abrupt variation of thermophysical properties or to multiple regions with markedly different geometrical sizes.

The present work further advances the integral transforms solution of heat transfer in heterogeneous media by implementing a symbolic-numerical computational algorithm for the analysis of transient three-dimensional heat conduction. The aim is to demonstrate the generality of this hybrid approach and the robustness and effectiveness of the associated algorithm in handling different classes of problems in terms of heterogeneities, under more involved unsteady multidimensional formulations and complex geometrical configurations. The Sturm-Liouville problem with arbitrarily space variable coefficients is solved by considering a fairly simple auxiliary eigenvalue problem with constant coefficients. Numerical results are here reported for three test cases. The first test case is associated with FGM (Functionally Graded Material) material which is here assumed to have its thermophysical properties represented by a three-dimensional spatially variable exponential functional behavior. The second test case is related to a heat conduction problem involving abrupt variations of thermophysical properties, as an illustration of a composite material with a substrate and different inclusions with spherical and cylindrical geometries, considered as the dispersed phase within the matrix. The last test case involves heat conduction in a complex physical configuration representative of an IGBT (Insulated Gate Bipolar Transistor) module [13,24,25], the most used static switches in power electronics applications, comprising multi-scale and multi-material arrangements. For each test case, a thorough convergence analysis is presented, so as to illustrate the integral transforms hybrid solution computational performance.

2. Problem formulation and solution methodology

The computational algorithm was built on the symbolic-numerical *Mathematica* platform [53], based on the following transient three-dimensional heat conduction formulation with space variable coefficients and linear or nonlinear source term:

$$w(x,y,z)\frac{\partial T(x,y,z,t)}{\partial t} = \nabla.\,[k(x,y,z)\nabla T(x,y,z,t)] - d(x,y,z)T(x,y,z,t) + g(x,y,z,t,T), \quad x_0 < x < x_1,\ \ y_0 < y < y_1,\ z_0 < z < z_1,\ \ t > 0 \tag{1.a}$$

with boundary conditions.

$$\alpha_{x,l}T(x_l,y,z,t) + (-1)^{l+1}\beta_{x,l}k(x_l,y,z)\frac{\partial T(x,y,z,t)}{\partial x}\bigg|_{x=x_l} = 0, \qquad l = 0,\ 1, \quad y_0 < y < y_1, \qquad z_0 < z < z_1, \qquad t > 0 \tag{1.b,c}$$

$$\alpha_{y,l}T(x,y_l,z,t) + (-1)^{l+1}\beta_{y,l}k(x,y_l,z)\frac{\partial T(x,y,z,t)}{\partial y}\bigg|_{y=y_l} = 0, \qquad l = 0,\ 1, \quad x_0 < x < x_1, \qquad z_0 < z < z_1, \qquad t > 0 \tag{1.d,e}$$

$$\alpha_{z,l}T(x,y,z_l,t) + (-1)^{l+1}\beta_{z,l}k(x,y,z_l)\frac{\partial T(x,y,z,t)}{\partial z}\bigg|_{z=z_l} = 0, \qquad l = 0,\ 1, \quad x_0 < x < x_1, \qquad y_0 < y < y_1, \qquad t > 0 \tag{1.f,g}$$

and initial condition

$$T(x,y,z,0) = f(x,y,z), \qquad x_0 \le x \le x_1, \qquad y_0 \le y \le y_1, \qquad z_0 \le z \le z_1 \tag{1.h}$$

The above formulation reflects that a filtering solution, either explicit or implicit, has already been applied so as to make the boundary conditions homogeneous in all the spatial coordinates. Also, it is sufficiently general to incorporate nonlinearities in the equation source terms, which can be originated from the source term itself or from nonlinear operators [35–43]. Following the formalism in the generalized integral transform technique (GITT), the integral transform pair is proposed as:

$$\overline{T}_i(t) = \int_{z=z_0}^{z_1}\int_{y=y_0}^{y_1}\int_{x=x_0}^{x_1} w(x,y,z)\,\widetilde{\psi}_i(x,y,z)\,T(x,y,z,t)\,dxdydz, \quad \textit{transform} \tag{2.a}$$

$$T(x,y,z,t) = \sum_{i=1}^{\infty}\widetilde{\psi}_i(x,y,z)\,\overline{T}_i(t), \quad \textit{inverse} \tag{2.b}$$

where the normalized eigenfunction and the normalization integral are given by.

$$\widetilde{\psi}_i(x,y,z) = \frac{\psi_i(x,y,z)}{\sqrt{N_i}}; \quad N_i = \int_{z=z_0}^{z_1}\int_{y=y_0}^{y_1}\int_{x=x_0}^{x_1} w(x,y,z)\psi_i^2(x,y,z)dxdydz \tag{3.a, b}$$

The eigenfunctions $\psi_i(x,y,z)$ and the corresponding eigenvalues μ_i can be evaluated from the following three-dimensional Sturm-Liouville problem:

$$\nabla.\,[k(x,y,z)\nabla\psi_i(x,y,z)] + [\mu_i^2 w(x,y,z) - d(x,y,z)]\psi_i(x,y,z) = 0 \tag{4.a}$$

$$\alpha_{x,l}\psi_i(x_l,y,z) + (-1)^{l+1}\beta_{x,l}k(x_l,y,z)\frac{\partial\psi_i(x,y,z)}{\partial x}\bigg|_{x=x_l} = 0, \qquad l = 0,\ 1, \quad y_0 < y < y_1, \qquad z_0 < z < z_1, \qquad t > 0 \tag{4.b,c}$$

$$\alpha_{y,l}\psi_i(x,y_l,z) + (-1)^{l+1}\beta_{y,l}k(x,y_l,z)\frac{\partial\psi_i(x,y,z)}{\partial y}\bigg|_{y=y_l} = 0, \qquad l = 0,\ 1, \quad x_0 < x < x_1, \qquad z_0 < z < z_1, \qquad t > 0 \tag{4.d,e}$$

$$\alpha_{z,l}\psi_i(x,y,z_l) + (-1)^{l+1}\beta_{z,l}k(x,y,z_l)\frac{\partial\psi_i(x,y,z)}{\partial z}\bigg|_{z=z_l} = 0,$$

$$l = 0,\ 1, \qquad x_0 < x < x_1, \qquad y_0 < y < y_1, \qquad t > 0 \tag{4.f,g}$$

The GITT can also be employed to solve the eigenvalue problem defined by Eqs. (4.a-g), based on a simpler auxiliary eigenvalue problem [37,40,44,45]. The simplest possible choice of auxiliary problem with constant coefficients has been here adopted, as will be seen in the examples to follow. The integral transformation of Eqs. (1.a-h) leads to the following transformed system:

$$\frac{d\overline{T}_i(t)}{dt} + \mu_i^2\overline{T}_i(t) = \overline{g}_i(t,\overline{T}_j(t)), \quad t > 0,\ i,j = 1,\ 2,\ 3,\ \ldots \tag{5.a}$$

$$\overline{T}_i(0) = \overline{f}_i = \int_{z=z_0}^{z_1}\int_{y=y_0}^{y_1}\int_{x=x_0}^{x_1} w(x,y,z)f(x,y,z)\widetilde{\psi}_i(x,y,z)dxdydz \tag{5.b}$$

where the transformed source term is given by

$$\overline{g}_i(t,\overline{T}_j(t)) = \int_{z=z_0}^{z_1}\int_{y=y_0}^{y_1}\int_{x=x_0}^{x_1} g(x,y,z,t,T)\widetilde{\psi}_i(x,y,z)dxdydz \tag{5.c}$$

The truncated nonlinear system (5) can be numerically solved for the transformed potentials employing the routine NDSolve from the *Mathematica* platform [53], with automatic control of absolute and relative errors, and the inverse formulae Eq. (2.b) is then recalled to analytically reconstruct the temperature field with respect to the space coordinates. For a linear source term, the temperature field can be obtained fully analytically by solving the decoupled system (5) and employing the inverse formulae Eq. (2.b), to yield:

$$T(x,y,z,t) = \sum_{i=1}^{\infty}\widetilde{\psi}_i(x,y,z)\left[\overline{f}_i\, e^{-\mu_i^2 t} + \int_0^t \overline{g}_i(t')e^{-\mu_i^2(t-t')}dt'\right] \tag{6}$$

An important part of the computational procedure is associated with the determination of the eigenvalues, μ_i, and corresponding three-dimensional eigenfunctions, $\psi_i(\mathbf{x}) = \psi_i(x,y,z)$, from the solution of the eigenvalue problem, Eqs. (4). In the proposed approach, all the information on the heterogeneity of the medium is accounted for by the eigenvalue problem through the space variable coefficients. One may briefly recall the solution procedure for eigenvalues problem through the GITT itself [37,40,44,45], rewriting problem (4) in the general form below:

$$\nabla.\,[k(\mathbf{x})\nabla\psi_i(\mathbf{x})] + [\mu_i^2 w(\mathbf{x}) - d(\mathbf{x})]\psi_i(\mathbf{x}) = 0, \quad \mathbf{x}\in V \tag{7.a}$$

with boundary conditions

$$\alpha(\mathbf{x})\psi_i(\mathbf{x}) + \beta(\mathbf{x})k(\mathbf{x})\frac{\partial\psi_i(\mathbf{x})}{\partial\boldsymbol{n}} = 0, \quad \mathbf{x}\in S \tag{7.b}$$

The idea is to solve problem (7) also employing the integral transform approach, but this time proposing an eigenfunction expansion for the unknown eigenfunctions themselves, $\psi_i(\mathbf{x})$. Thus, a simpler auxiliary eigenvalue problem with known analytical solution needs to be defined, usually based on characteristic simplified functional forms of the space variable coefficients, which is given in general terms by:

$$\nabla.\,[\widehat{k}(\mathbf{x})\nabla\Omega_n(\mathbf{x})] + [\lambda_n^2\widehat{w}(\mathbf{x}) - \widehat{d}(\mathbf{x})]\Omega_n(\mathbf{x}) = 0, \quad \mathbf{x}\in V \tag{8.a}$$

$$\alpha(x)\Omega_n(\mathbf{x}) + \beta(\mathbf{x})\widehat{k}(\mathbf{x})\frac{\partial\Omega_n(\mathbf{x})}{\partial\boldsymbol{n}} = 0, \quad \mathbf{x}\in S \tag{8.b}$$

where the coefficients, $\widehat{w}(\mathbf{x})$, $\widehat{k}(\mathbf{x})$, $\widehat{d}(\mathbf{x})$, are simpler coefficients, characteristic of the original ones, that allow for an analytical solution of the auxiliary problem, yielding the auxiliary eigenfunctions, $\Omega_n(\mathbf{x})$, and corresponding eigenvalues, λ_n. Then, the integral transform pair for solving problem (7) is given as:

$$\overline{\psi}_{i,n} = \int_V \widehat{w}(\mathbf{x})\psi_i(\mathbf{x})\widetilde{\Omega}_n(\mathbf{x})dv, \quad \textit{Transform} \tag{9.a}$$

$$\psi_i(\mathbf{x}) = \sum_{n=1}^{\infty}\widetilde{\Omega}_n(\mathbf{x})\overline{\psi}_{i,n}, \quad \textit{Inverse} \tag{9.b}$$

The integral transformation of problem (7) is accomplished through the operator $\int_V \widetilde{\Omega}_n(\mathbf{x})(.)dv$, resulting in an algebraic eigenvalue problem:

$$(\mathbf{A} + \mathbf{C})\{\overline{\psi}\} = \mu^2\mathbf{B}\{\overline{\psi}\} \tag{10.a}$$

where the elements of the coefficients matrices above are given by [40]:

$$A_{ij} = \int_S \frac{\widetilde{\Omega}_i(\mathbf{x}) - \widehat{k}(\mathbf{x})\frac{\partial\widetilde{\Omega}_i(\mathbf{x})}{\partial\boldsymbol{n}}}{\alpha(\mathbf{x}) + \beta(\mathbf{x})}\left[\beta(\mathbf{x})(k(\mathbf{x}) - \widehat{k}(\mathbf{x}))\frac{\partial\widetilde{\Omega}_j(\mathbf{x})}{\partial\boldsymbol{n}}\right]ds -$$
$$- \int_S (k(\mathbf{x}) - \widehat{k}(\mathbf{x}))\widetilde{\Omega}_i(\mathbf{x})\frac{\partial\widetilde{\Omega}_j(\mathbf{x})}{\partial\boldsymbol{n}}ds + \int_V (k(\mathbf{x}) - \widehat{k}(\mathbf{x}))\nabla\widetilde{\Omega}_i(\mathbf{x}).\,\nabla\widetilde{\Omega}_j(\mathbf{x})dv +$$
$$+ \int_V (d(\mathbf{x}) - \widehat{d}(\mathbf{x}))\widetilde{\Omega}_i(\mathbf{x})\widetilde{\Omega}_j(\mathbf{x})dv \tag{10.b}$$

$$C_{ij} = \lambda_i^2\delta_{ij} \tag{10.c}$$

$$B_{ij} = \int_V w(\mathbf{x})\widetilde{\Omega}_i(\mathbf{x})\widetilde{\Omega}_j(\mathbf{x})dv \tag{10.d}$$

where δ_{ij} is the Kronecker delta.

The numerical solution of the algebraic eigenvalue problem (10) provides the eigenvalues and eigenvectors that permit the reconstruction of the original eigenfunction through the inversion formula (9.b). Again, symbolic computation is employed in the evaluation of the integral transformation coefficients in Eqs. (10.b, d) [53]. The analytical solution of the auxiliary eigenvalue problem, Eqs.(8), is in general achieved through separation of variables. The eigenfunction expansions for the original eigenvalue problem are then written as a reordered single summation comprising the contributions of the auxiliary eigenfunctions in each spatial direction. A reordering scheme needs to be adopted so as to reduce the order of the truncated algebraic system to a reasonable size, i.e., defining the truncated system that most closely represents the infinite one. The use of the squared eigenvalues criterium is the most frequently employed one, though other criteria can be invoked, such as the diagonal of the transformed coefficients matrix, according to the individual contribution in the final result [38–41,54]. Also, convergence acceleration techniques can be recalled for improved computational performance, whenever required [55]. It should be recalled that there are two convergence behaviors to be analyzed in each application, one related to the eigenvalue problem expansion, Eq. (9.b), where a truncation order N_T will be considered, and for the temperature expansion, Eq. (6), for which the infinite series will be truncated at order M_T in the results section. The analytic nature of the approach allows for the determination of pre-estimates of the required truncation orders for a certain desired accuracy level. For instance, in the case of the eigenvalue problem expansion, the diagonal form of system (10.a) can provide an approximate solution that serves this estimation purpose, while the linearized version of Eq. (5.a) leads to a convergence behavior estimate of the temperature expansion. In the results that follow, convergence shall be independently examined for the eigenvalue problem and temperature field expansions.

3. Test cases

3.1. Heat conduction in FGMs (functionally graded materials)

The GITT approach is first demonstrated in the solution of transient three-dimensional heat conduction problems in heterogeneous media with continuously but markedly variable thermophysical properties, such as in the case of functionally graded materials (FGMs), leading to the solution of the corresponding three-dimensional Sturm-Liouville

problem with space variable coefficients. Thus, the first test case deals with heat conduction defined in a parallelepiped region with thermophysical properties steeply and simultaneously varying in all three directions (x, y, and z), governed by Eqs. (1) in dimensionless form. The coefficients of Eqs. (1.a-h) and the boundary coefficients present in Eqs. (1)–(4) are given in the selected test case by:

$$k(x,y,z) = k_0 e^{[2b(x+y+z)]}, \quad w(x,y,z) = w_0 e^{[2b(x+y+z)]}, \quad d(x,y,z) = 0, \quad f(x,y,z) = 1, \quad g(x,y,z,t,T) = 0$$

$$\alpha_{x,0} = \alpha_{y,0} = \alpha_{z,0} = 0, \quad \beta_{x,0} = \beta_{y,0} = \beta_{z,0} = 1, \; \alpha_{x,1} = \alpha_{y,1} = \alpha_{z,1} = 1, \; \beta_{x,1} = \beta_{y,1} = \beta_{z,1} = 0 \tag{11.a-j}$$

where the required numerical coefficients are $k_o = 1$, $w_o = 10$, b = 1 [12].

3.2. Heat conduction in a composite with spherical and cylindrical inclusions

The second test case deals with heat conduction in a heterogeneous medium related to multiple non-contacting three-dimensional inclusions within a matrix filler, where spherical and cylindrical structures are considered as dispersed elements of known physical properties. The physical model of the second test case is shown in Fig. 1. As can be observed, the central cylinder is rotated of 45° with respect to the vertical axis z. The thermophysical properties for the single domain formulation and the boundary coefficients are given by:

$$w(x,y,z), \quad k(x,y,z) = \begin{cases} w_1, & k_1, \\ \text{Cylinders} & \text{and} \quad \text{Spheres (dispersed phase)} \\ w_2, & k_2, \quad \text{Parallelepiped (continuum phase)} \end{cases}$$

$$\alpha_{x,0} = \alpha_{y,0} = \alpha_{z,0} = 0, \quad \beta_{x,0} = \beta_{y,0} = \beta_{z,0} = 1, \quad \alpha_{x,1} = \alpha_{y,1} = \alpha_{z,1} = 1, \quad \beta_{x,1} = \beta_{y,1} = \beta_{z,1} = 0 \tag{12.a-f}$$

The dimensions of the parallelepiped (matrix phase) were chosen as: $L_x = 0.2$ m, $L_y = 0.1$ m and $L_z = 0.05$ m. Furthermore, the dimensions of the dispersed elements are presented in Tables 1 and 2. Table 3 shows the thermophysical properties of the materials used in this test case. The parallelepiped matrix phase is composed of a copper-aluminum alloy, while the cylindrical and spherical dispersed phases are of duralumin, which is a well-known light and strong aluminum alloy containing 3.5–4.5% of copper and small quantities of silicon, magnesium, and manganese, quite common in aircraft manufacturing.

Table 1
Dimensions of the cylindrical inclusions.

Cylinder	Height (mm)	Radius (mm)	z-angle	Position (x,y,z) mm
1	30	8	45°	(100,50,15)
2	30	7	0	(85,75,25)
3	40	10	0	(25,25,25)
4	20	5	0	(150,25,25)

Table 2
Dimensions of the spherical inclusions.

Sphere	Radius (mm)	Position (x,y,z) mm
1	8	(150,75,25)
2	8	(50,75,25)
3	6	(110,25,25)

3.3. Heat conduction in IGBT (insulated gate bipolar transistor) module

The third test case is related to heat transfer in a physical model of an IGBT (Insulated Gate Bipolar Transistor) module. The reliability of this semiconductor device is closely linked to the operating junction temperatures of the IGBT and the diode chips present in it. It can be noted that the IGBT module, in its actual design (Fig. 2), has a complex multi-scale and multi-material geometry. Fig. 2 presents an opened IGBT module disconnected from the plastic case to allow for the inside view. In the present methodological demonstration, a simpler geometry is considered (Fig. 3), maintaining the different materials with physical properties varying along the three coordinate directions, and analyzing the intrinsic transient behavior with the heat source in one of the layers, as shown in Fig. (3a–c). The properties of each material that compose the IGBT module simulated in the present work are shown in Table 4.

All boundary conditions are of the third kind, thus the boundary condition coefficients were defined as:

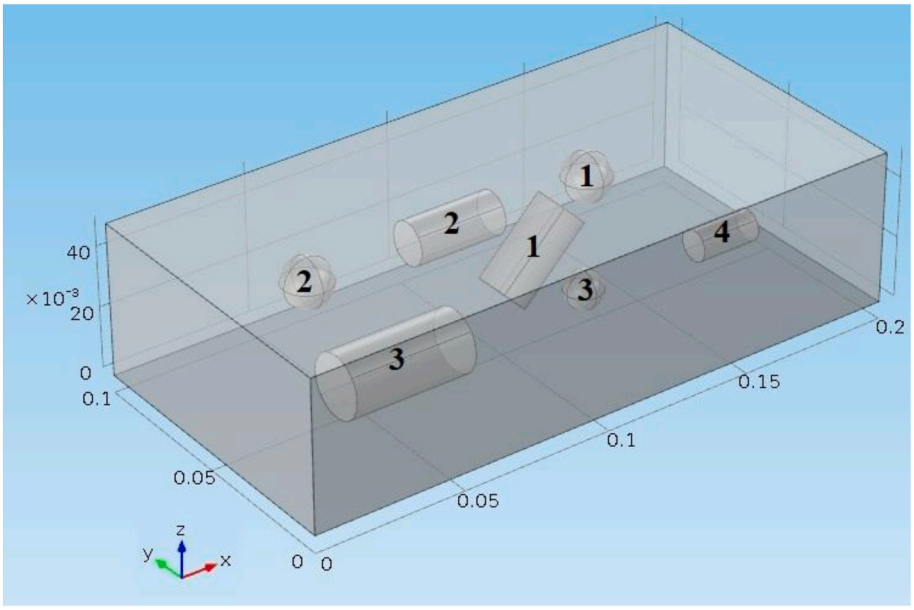

Fig. 1. Schematic representation of the composite medium for test case 2, consisting of dispersed elements formed by three spheres and four cylinders encapsulated by a parallelepiped matrix.

Table 3
Thermophysical properties and initial conditions of the composite consisting of metallic dispersed elements formed by three spheres and four cylinders surrounded by a metal matrix.

Component	Materials	Composition	$k\left(\frac{W}{m\,K}\right)$	$w \times 10^6\left(\frac{J}{m^3 K}\right)$	Initial Temp. (°C)
Dispersed	Duralumin	94–96% Al, 3–5% Cu trace Mg	164	2.32	50
Matrix	Copper-aluminum alloy	95% Cu, 5% Al	83	3.55	50

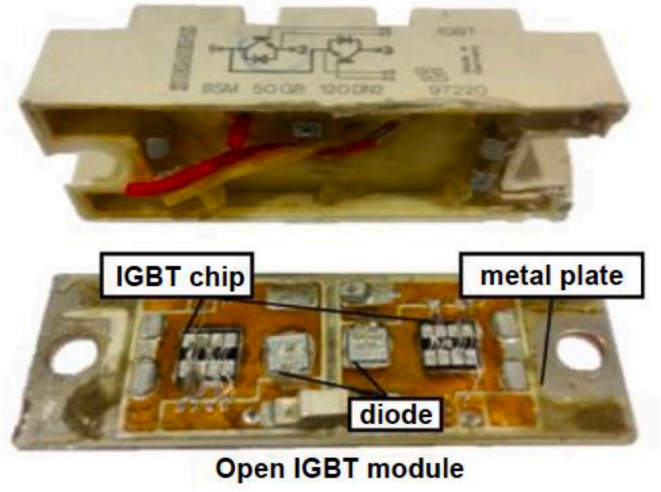

Fig. 2. Real IGBT module (Dual module Siemens BSM 50GB 120DN2), opened and disconnected from the plastic case [24].

$$\alpha_{x,0} = \alpha_{x,1} = h_x, \quad \alpha_{y,0} = \alpha_{y,1} = h_y, \quad \alpha_{z,0} = \alpha_{z,1} = h_z,$$
$$\beta_{x,0} = \beta_{y,0} = \beta_{z,0} = -1, \quad \beta_{x,1} = \beta_{y,1} = \beta_{z,1} = 1 \tag{13.a-e}$$

From the above coefficients, Eqs. (1) are rewritten, after application of a simple filter for the external ambient temperature, as:

$$w(x,y,z)\frac{\partial T(x,y,z,t)}{\partial t} = \nabla.\,(k(x,y,z)\nabla T) + g(x,y,z),$$
$$0 < x < L_x, \quad 0 < y < L_y, \quad 0 < z < L_z, \; t > 0 \tag{14.a}$$

$$-k_1\frac{\partial T}{\partial x} + h_x T = 0, \quad x = 0, \quad 0 < y < L_y, \quad 0 < z < L_z, \quad t > 0 \tag{14.b}$$

$$k_1\frac{\partial T}{\partial x} + h_x T = 0, \quad x = L_x, \quad 0 < y < L_y, \quad 0 < z < L_z, \quad t > 0 \tag{14.c}$$

$$-k_1\frac{\partial T}{\partial y} + h_y T = 0, \quad y = 0, \quad 0 < x < L_x, \quad 0 < z < L_z, \quad t > 0 \tag{14.d}$$

$$k_1\frac{\partial T}{\partial y} + h_y T = 0, \quad y = L_y, \quad 0 < x < L_x, \quad 0 < z < L_z, \quad t > 0 \tag{14.e}$$

$$-k_4\frac{\partial T}{\partial z} + h_z T = 0, \quad z = 0, \quad 0 < x < L_x, \quad 0 < y < L_y, \quad t > 0 \tag{14.f}$$

$$k_1\frac{\partial T}{\partial z} + h_z T = 0, \quad z = L_z, \quad 0 < x < L_x, \quad 0 < y < L_y, \quad t > 0 \tag{14.g}$$

$$T(x,y,z,0) = f(x,y,z) - T_\infty, \quad 0 \le x \le L_x, \quad 0 \le y \le L_y, \quad 0 \le z \le L_z \tag{14.h}$$

where,
$h_x = h_y = h_z = 5\,\frac{W}{m^2 K}$, $f(x,y,z) = T_\infty$, $k_1 = k_{Si3N4} = 40\,\frac{W}{m\,K}$, $k_4 = k_{AlSiC9} = 180\,\frac{W}{m\,K}$ and $g(x,y,z) = 10^8\,\frac{W}{m^3}$ is the source term located on the silicon layer, indicated by the red component 2 in Fig. 3a.

It is worth mentioning that in cases 2 and 3 here analyzed it was assumed a perfect thermal contact among the subregions, although it is not a limitation of the approach. Any thermal interface resistance, can be included just by adding this information in the variable coefficients through a fictitious layer, as described in [49].

4. Results

4.1. Heat conduction in FGM (functionally graded materials)

This problem was solved in dimensionless form, with the dimensions of the domain chosen as $L_x = L_y = L_z = 1$ and the values for the coefficients as $k_0 = 1$, $w_0 = 10$, b = 1. Fig. 4a,b illustrate the variation of these dimensionless thermophysical properties along the (x,y) domain for fixed z = 1. We note that a significantly large ratio of approximately 400 times is achieved between the values of the coefficients k(x,y,z) and w(x,y,z) in opposite boundaries.

Table 5 illustrates the convergence behavior of the eigenvalues solved by GITT in this first test case. Each line shows a different eigenvalue order, while the columns refer to increasing truncation orders in the auxiliary eigenfunction expansions, Eq. (9.b). One can observe full convergence to all five significant digits shown, for truncation orders of the eigenvalue problem (N_T) up to 230 terms.

As an additional illustration of the eigenvalues convergence, Fig. 5 shows the estimated relative deviations on specific eigenvalues, with respect to the most precise eigenvalue evaluated, for increasing truncation orders. For truncation orders (N_T) less than 200 terms, the estimated relative deviations on the selected eigenvalues were less than 0.01%, indicating the excellent convergence attained in the solution of the eigenvalue problem with space variable coefficients. These relative deviations were calculated with respect to the highest truncation order shown in Table 5 above, $N_T = 230$, according to:

$$\epsilon_\mu = \left|\frac{\mu_n - \mu_{n_{\max}}}{\mu_{n_{\max}}}\right| .100 \tag{15}$$

where $\mu_{n_{\max}}$ represents the eigenvalue computed with truncation order $N_T = 230$, the largest truncation order here adopted, which approximates the unavailable exact solution.

Table 6 illustrates the temperature convergence analysis for different values of the coordinate x, and fixed values of the other independent variables, namely, y = 0.4, z = 0.4, and $t = 0.2$, where M_T is the truncation order for the temperature expansion. One can observe that four significant digits are converged in all axial positions. Also, it can be verified the adherence to at least two significant digits when comparing the hybrid solution via GITT against the fully numerical solution obtained via the *NDSolve* routine of *Mathematica* 11.3 [53], in its default mode that considers an automatic error control of eight digits for the local absolute or relative errors allowed for in each step of the numerical solution, respectively, the *AccuracyGoal* and *PrecisionGoal* controllers [53]. The largest relative deviation in the evaluated temperature values was 0.19%, as compared to the GITT solution with 190 terms in the temperature expansion and 200 terms in the expansion for the eigenvalue problem. The comparison between the hybrid (GITT) and numerical (NDSolve) solutions is also shown in Fig. 6, where an excellent agreement is demonstrated to the graph scale, for two different times ($t = 0.3$ and $t = 0.6$), along the x coordinate.

(a)

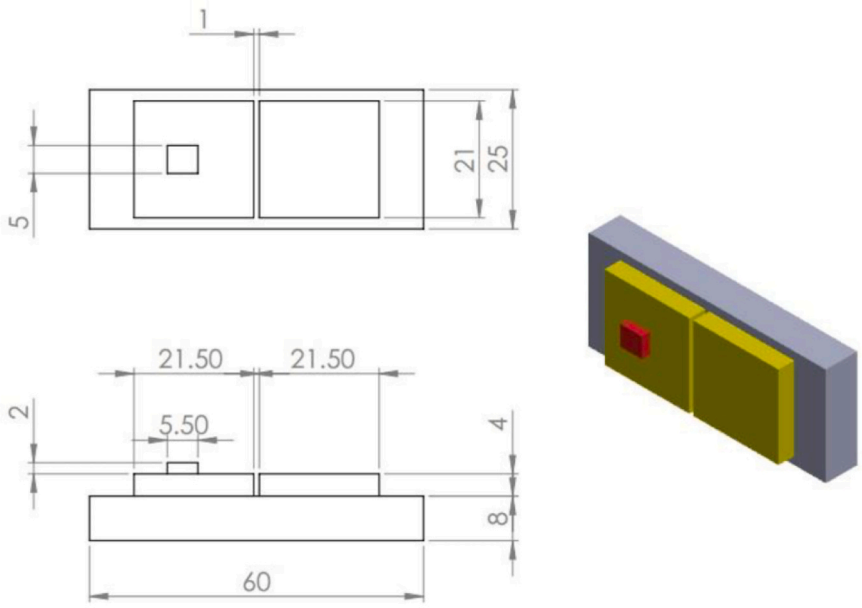

(b)

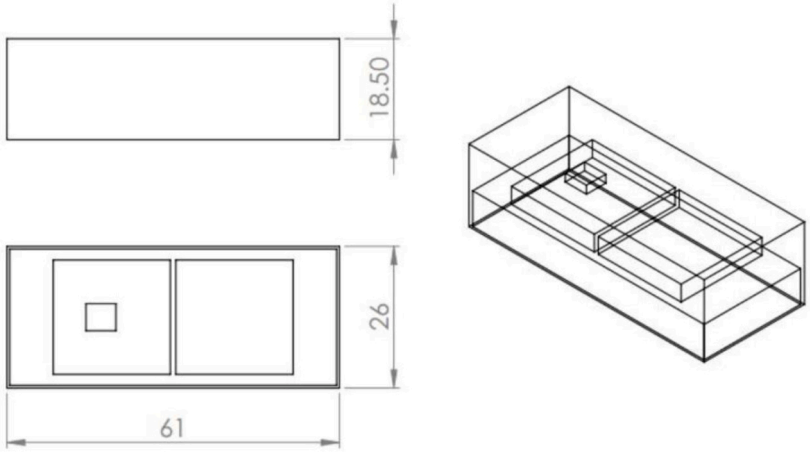

(c)

Fig. 3. Different views of the physical model adopted for test case 3 (dimensions in mm) [24]: (a) Cross section; (b) IGBT layers dimensions; (c) IGBT Si_3N_4 layer quotas;

Table 4
Properties of the various layers of the IGBT module [24].

Component	Material	Density (kg/m^3)	Thermal conductivity (W/mK)	Heat capacity (J/m^{3}K)
1	Silicon Nitride (Si_3N_4)	3250	40	710
2	Silicon (Si)	2329	120	712
3	Aluminum nitrate (AlN)	3259.8	170	740
4	$AlSiC_9$	3000	180	434

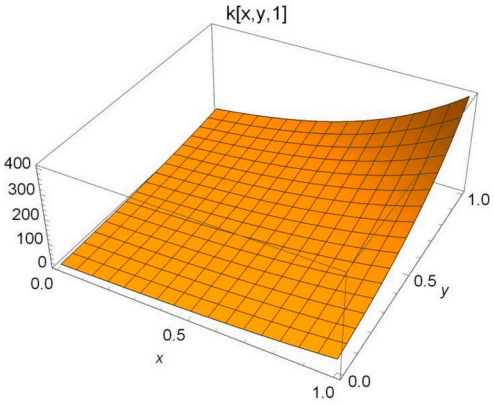

a. Variation of the dimensionless thermal conductivity coefficient $k(x,y,z)$ for the FGM example (test case 1) at z = 1.

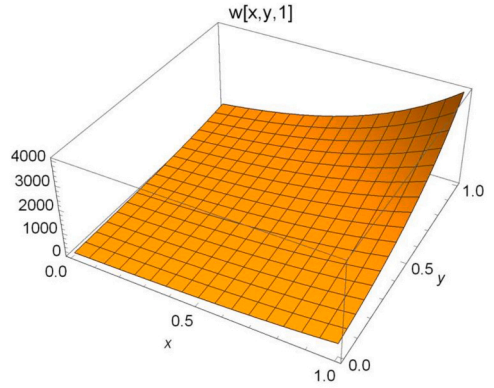

b. Variation of the dimensionless thermal capacity coefficient $w(x,y,z)$ for the FGM example (test case 1) at z = 1.

Fig. 4. (a) Variation of the dimensionless thermal conductivity coefficient $k(x,y,z)$ for the FGM example (test case 1) at z = 1. (b) Variation of the dimensionless thermal capacity coefficient $w(x,y,z)$ for the FGM example (test case 1) at z = 1.

4.2. Heat conduction in a composite with spherical and cylindrical inclusions

The physical model employed in this test case requires to evaluate integrations in each individual inclusion and in the overall matrix region so as to compute the required integral transformation coefficients. To perform an integration in a specific region, either numerical or analytical, the *Mathematica* platform performs a change of variables and remaps this region over a unit cube, which can be integrated with the method *MultiDimensionalRule* from the *Mathematica* system [53]. In order to use the numerical or analytical integration routines, it is then necessary to create a region through the command *Region* [53]. In this case, three distinct regions were created, the first one in the form of cylinders, the second in the form of spheres, and the third one related to the overall parallelepiped region. The coefficients of the algebraic matrix eigenvalue problem were determined by integrating analytically in the parallelepiped region, encompassing the spherical and cylindrical regions, and numerically in the spherical and cylindrical regions. After that, the subtraction of these results is performed, recalling the properties of each material. In this second test case, the solution obtained through GITT was critically compared with the purely numerical solution obtained via the COMSOL Multiphysics 4.4 software [56]. In the

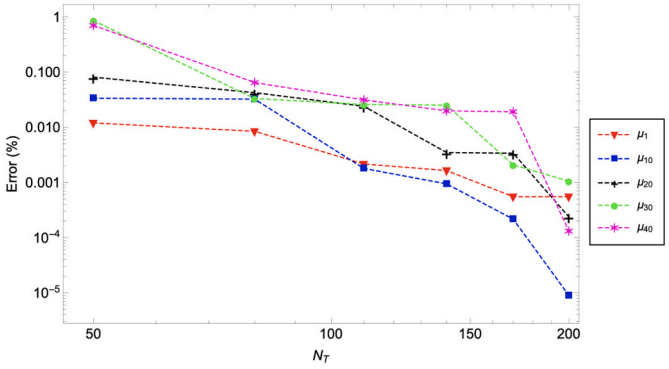

Fig. 5. Relative deviations of 1st, 10th, 20th, 30th, and 40th eigenvalues associated with the eigenvalue problem with space variable coefficients for the FGM application (test case 1) with respect to the best estimate with the largest truncation order, $N_T = 230$.

Table 6
Temperature convergence along the dimensionless axial coordinate x, at y = 0.4, z = 0.4 and t = 0.2, using 200 terms in the eigenvalue problem expansion, for FGM application (test-case 1).

	T(x,0.4,0.4,0.2)			
M_T	0.2	0.4	0.6	0.8
10	0.8733	0.9645	1.0031	0.6456
40	0.9899	0.9805	0.9226	0.6057
70	0.9922	0.9916	0.9256	0.6116
100	0.9926	0.9873	0.9246	0.6110
130	0.9926	0.9879	0.9246	0.6111
160	0.9925	0.9879	0.9246	0.6110
190	0.9925	0.9879	0.9246	0.6110
Numerical (NDSolve) [53]	0.9903	0.9856	0.9242	0.6108
Deviation (%)	0.19	0.18	0.035	0.0084

Table 5
Convergence analysis of the eigenvalues obtained through GITT for the FGM application (test case 1).

μ_i	$N_T = 50$	$N_T = 80$	$N_T = 110$	$N_T = 140$	$N_T = 170$	$N_T = 200$	$N_T = 230$
1	1.2390	1.2390	1.2389	1.2389	1.2389	1.2389	1.2389
2	1.8810	1.8810	1.8809	1.8808	1.8808	1.8808	1.8808
3	1.8816	1.8810	1.8809	1.8809	1.8808	1.8808	1.8808
4	1.8816	1.8810	1.8809	1.8809	1.8808	1.8808	1.8808
5	2.3549	2.3539	2.3539	2.3539	2.3537	2.3537	2.3537
6	2.3549	2.3539	2.3539	2.3539	2.3537	2.3537	2.3537
7	2.3549	2.3539	2.3539	2.3539	2.3537	2.3537	2.3537
8	2.7378	2.7378	2.7369	2.7369	2.7369	2.7369	2.7367
9	2.7378	2.7378	2.7369	2.7369	2.7369	2.7369	2.7369
10	2.7378	2.7378	2.7369	2.7369	2.7369	2.7369	2.7369
20	3.3933	3.3920	3.3913	3.3906	3.3906	3.3905	3.3905
30	3.9601	3.9277	3.9275	3.9274	3.9265	3.9265	3.9265
40	4.4319	4.4040	4.4025	4.4020	4.4020	4.4012	4.4011

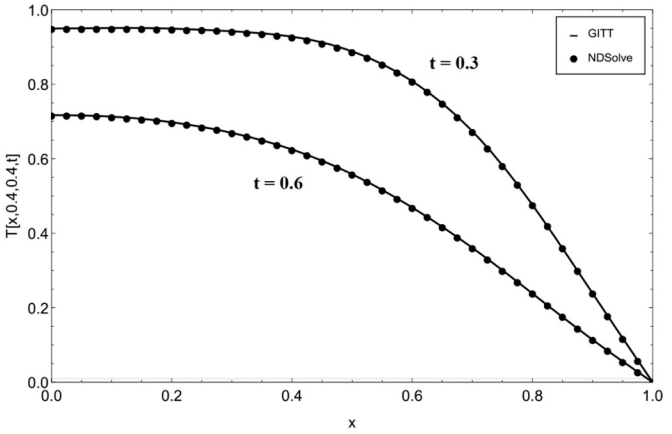

Fig. 6. Comparison between the GITT solution (using 200 terms in the eigenvalue problem and 70 terms in the temperature expansion) and the fully numerical solution (NDSolve [53]), along the x coordinate, at y = 0.4, z = 0.4, for times t = 0.3 and t = 0.6, for FGM application (test-case 1).

Table 7
Maximum mesh element size and number of elements for composite medium example (test case 2) used in the numerical COMSOL solution [56].

Maximum element size (mm)	Total number of elements in the domain
30	11,533
20	20,584
16	32,794
11	51,956

COMSOL numerical simulations, the relative and absolute tolerances were set to the values of 10^{-3} and 10^{-4}, respectively. Moreover, the mesh in COMSOL was built with the automatic mesh control, informing only the maximum element size of the generated mesh. Table 7 summarizes the tested meshes maximum sizes and the number of elements utilized in each numerical simulation.

Fig. 7 shows the selected testing positions within the domain represented by the red line along x, at y = 75 mm, z = 25 mm, that shall base the comparisons that follow. Fig. 8 illustrates the graphical convergence of the numerical solution [56], along the red line of Fig. 7, employing different values of the maximum mesh size, from 11 to 30 mm.

Fig. 9 illustrates the finite element mesh with a maximum element size of 30 mm used in the present simulations using the COMSOL platform [56].

Table 8 illustrates the convergence analysis of the eigenvalue problem solved by GITT for the composite example (test case 2). One can

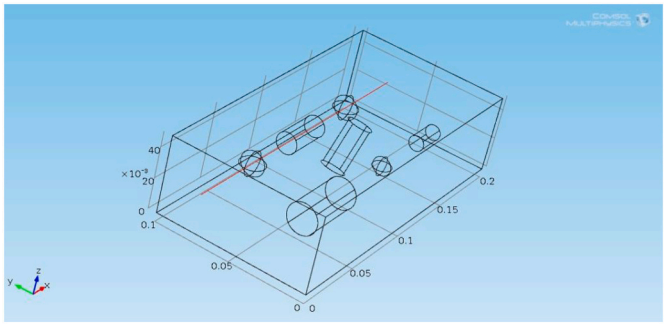

Fig. 7. Red line indicating the region of the domain along x, for y = 75 mm and z = 25 mm, employed in the comparisons for the composite example (test case 2). (For interpretation of the references to colour in this figure legend, the reader is referred to the web version of this article.)

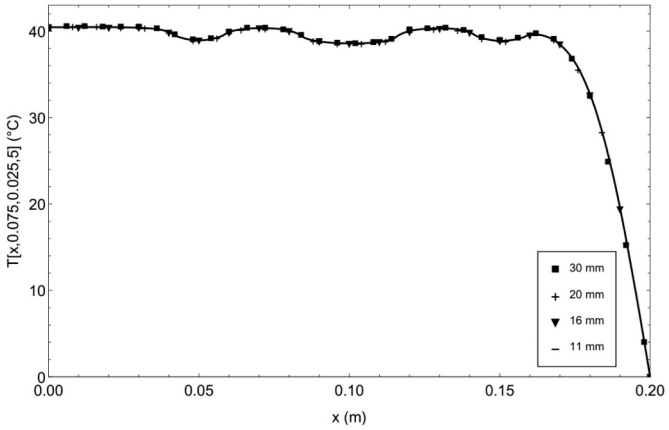

Fig. 8. Numerical solution [56] for different maximum mesh sizes, at the point y = 75 mm, z = 25 mm, and t = 5 s, for composite example (test case 2).

notice the convergence to four significant digits for the selected eigenvalues at a truncation order of at most N_T = 320. Fig. 10 shows another illustration of the eigenvalues convergence rates in the composite medium example, through the decrease on the relative deviations of the eigenvalues for increasing truncation orders in the auxiliary eigenfunction expansions. For truncation orders (N_T) less than 260 terms, the relative deviations were already less than 0.05%, indicating the excellent convergence rates for the eigenvalue problem. These relative deviations were calculated with respect to the largest truncation order of the expansions, that is, for N_T = 320, according to Eq. (15). Table 9 presents the convergence of the temperature field for different values of x, at y = 75 mm, z = 25 mm, and t = 5 s, where M_T is the truncation order of the temperature expansions. One can notice three fully converged significant digits in all axial positions presented. The largest relative deviation with respect to the COMSOL simulation, in all the evaluated positions, was 1.44% using 260 terms in the expansion for the eigenvalue problem. The excellent agreement between the hybrid (GITT) and numerical (COMSOL) solutions can also be visualized to the graphical scale in Fig. 11, along the coordinate x, at y = 75 mm, z = 25 mm, and for times t = 5 s and t = 10 s. The GITT solution here employed 260 terms for the eigenvalue problem and 220 terms for the temperature expansion.

4.3. Heat conduction in IGBT (insulated gate bipolar transistor) module

Th IGBT device is basically a power semiconductor device primarily used as an electronic switch, which combines high current density with fast switching. The current flow in these devices induces fast temperature increase inside the module by Joule effect and the temperature has to be controlled not to exceed a maximum pre-established value. Numerical simulation is then the engineering tool for thermal

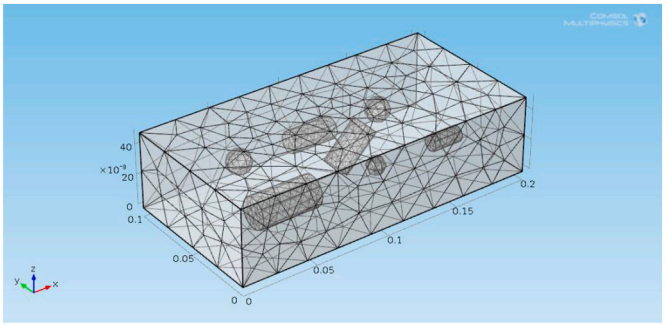

Fig. 9. Final configuration of the mesh with maximum element size of 30 mm [56] for composite example (test case 2).

Table 8
Convergence analysis of the eigenvalues obtained through GITT for composite example (test case 2).

μ_i	N_T = 80	N_T = 140	N_T = 200	N_T = 260	N_T = 320
1	0.1784	0.1783	0.1782	0.1782	0.1782
2	0.2083	0.2082	0.2082	0.2081	0.2081
3	0.2595	0.2594	0.2593	0.2593	0.2593
4	0.2824	0.2821	0.2820	0.2819	0.2819
5	0.3013	0.3012	0.3011	0.3010	0.3010
6	0.3218	0.3216	0.3215	0.3214	0.3214
7	0.3379	0.3377	0.3376	0.3376	0.3375
8	0.3875	0.3873	0.3871	0.3871	0.3870
9	0.3905	0.3900	0.3898	0.3896	0.3896
10	0.4198	0.4193	0.4190	0.4188	0.4187
20	0.5194	0.5190	0.5187	0.5186	0.5185
30	0.5874	0.5865	0.5859	0.5855	0.5853
40	0.6425	0.6415	0.6411	0.6409	0.6407

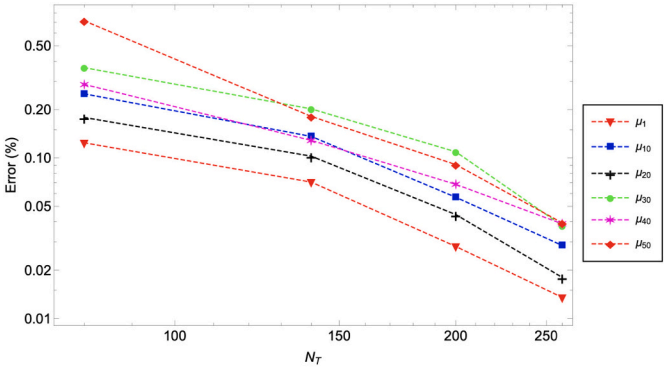

Fig. 10. Estimated relative deviations of the 1st, 10th, 20th, 30th, 40th and 50th eigenvalues of the composite example (test case 2) eigenvalue problem with respect to the best estimate with the largest truncation order, N_T = 320.

Table 9
Temperature convergence along the axial coordinate x, at y = 75 mm, z = 25 mm and t = 5 s, using 260 terms in the auxiliary eigenfunction expansion for the composite example (test case 2).

	T(x, 0.075, 0.025, 5)					
M_T	0.03	0.06	0.09	0.12	0.15	0.18
10	36.96	36.36	34.16	33.60	35.22	22.52
40	41.15	40.32	39.83	40.79	40.05	32.60
70	40.61	40.17	39.72	40.31	39.75	33.11
100	40.35	39.87	39.44	39.97	39.48	32.77
130	40.32	39.87	39.39	39.94	39.56	32.71
160	40.28	39.83	39.38	39.92	39.54	32.65
190	40.27	39.81	39.38	39.91	39.53	32.63
220	40.27	39.80	39.37	39.91	39.52	32.62
250	40.27	39.80	39.37	39.90	39.51	32.62
Numerical [56]	40.47	39.90	38.81	39.98	38.88	32.75
Deviation (%)	0.49	0.24	1.44	0.19	1.64	0.38

management design, with the maximum temperature value at the module being the criterium to establish the operating work range of the device.

As in the previous case, four types of tetrahedral meshes were tested in the fully numerical solution analysis [56]. Table 10 shows the maximum size and number of elements in the computational domain for each run.

Fig. 12 shows an example of the temperature profiles obtained through COMSOL [56] for the four mesh configurations shown in Table 10, with a source term g = 10^8 W/m^3. Note that for maximum sizes of mesh elements less than 6.10 mm, the solution remains practically unchanged to the graph scale. It can be noticed that the region most directly affected by heat generation term requires a more refined

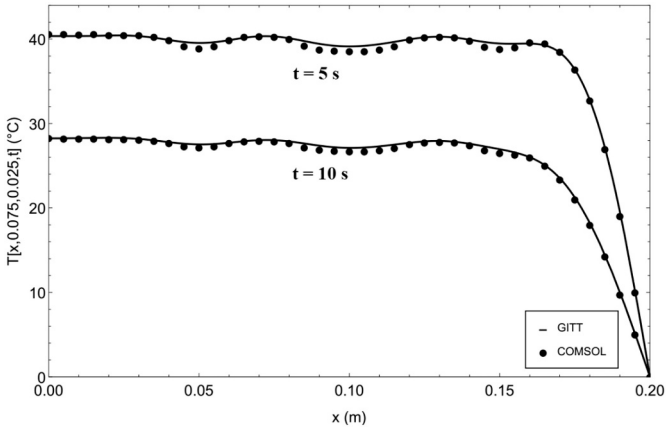

Fig. 11. Comparison between the hybrid (GITT) and numerical (COMSOL [56]) solutions for composite example (test case 2), along the x coordinate, at y = 75 mm, z = 25 mm, and for times t = 5 s and t = 10 s.

Table 10
Maximum size and quantity of elements used in the numerical solution with COMSOL [56] for the domain of the IGBT module (test case 3).

Maximum element size (mm)	Total number of elements in the domain
9.15	13,036
6.10	33,159
4.88	59,655
3.35	90,224

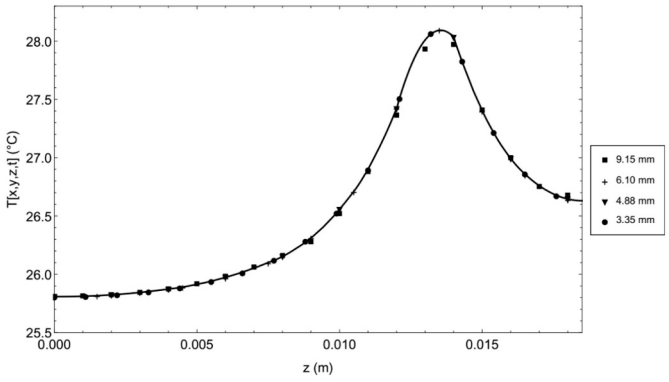

Fig. 12. Graphical convergence of the COMSOL numerical solution [56] for the temperature distribution along z, for the four mesh configurations in Table 10, with x = 16.5 mm, y = 12.5 mm and t = 5 s for the IGBT module (test case 3) with g = 10^8 W/m^3.

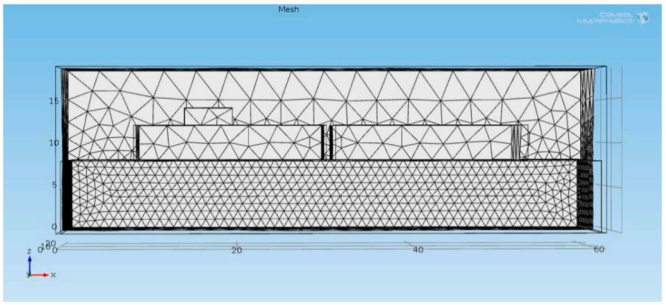

Fig. 13. Final arrangement of the mesh elements (maximum size of the element equal to 6.10 mm) for the COMSOL [56] numerical solution of the IGBT module (test case 3).

Table 11
Convergence analysis of the eigenvalues obtained through GITT for the IGBT module (test case 3).

μ_i	N_T										
	200	300	400	500	600	700	800	900	1000	1100	1200
20	1.463	1.455	1.453	1.452	1.452	1.451	1.448	1.443	1.442	1.442	1.441
40	2.034	2.008	2.002	1.999	1.998	1.998	1.995	1.994	1.989	1.989	1.988
60	2.418	2.343	2.334	2.328	2.325	2.322	2.320	2.319	2.319	2.318	2.318
80	2.872	2.651	2.611	2.605	2.603	2.602	2.601	2.601	2.601	2.601	2.601
100	3.295	2.976	2.867	2.821	2.819	2.816	2.811	2.805	2.801	2.801	2.801
120	4.150	3.364	3.139	3.096	3.079	3.074	3.066	3.065	3.065	3.063	3.063
140	4.665	3.691	3.396	3.276	3.242	3.222	3.217	3.216	3.215	3.212	3.212
160	5.310	4.200	3.648	3.502	3.422	3.394	3.380	3.369	3.362	3.359	3.358
180	6.030	4.777	4.032	3.673	3.609	3.579	3.555	3.543	3.518	3.513	3.510
200	6.866	5.409	4.429	4.005	3.793	3.713	3.686	3.681	3.669	3.667	3.663

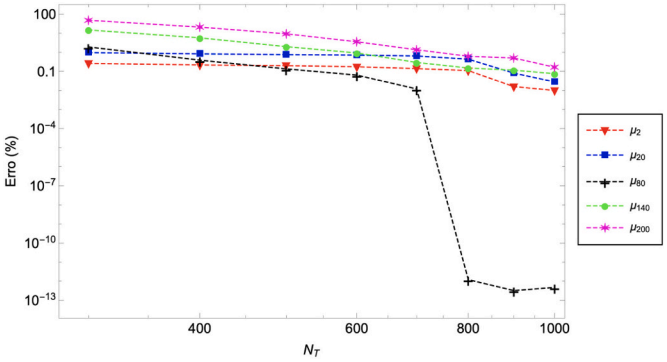

Fig. 14. Estimated relative deviations of the 2nd, 20th, 80th, 140th, and 200th eigenvalues of the IGBT module (test case 3) eigenvalue problem.

mesh for a more evident convergence to the graph scale. Fig. 13 illustrates the mesh elements distribution for the case when the maximum element size was 6.10 mm, while in this case the minimum size of the mesh elements was 1.1 mm.

Table 11 illustrates the convergence behavior of the eigenvalue problem solved by GITT for the IGBT module (test case 3). Although one can notice convergence to four significant digits for most of the selected eigenvalues at a truncation order of at most $N_T = 1200$, it can be observed that the higher order eigenvalues might require a few additional terms, being however fully converged to three digits within the present truncation orders.

Fig. 14 shows the decrease on the relative deviations of the eigenvalues for increasing truncation orders in the auxiliary eigenfunction expansions. For truncation orders (N_T) less than 1000 terms, the relative deviations are already less than 1%. These deviations were calculated with respect to the eigenvalues computed with the largest truncation order for the expansions, that is, for $N_T = 1200$, according to Eq. (15).

In order to report the convergence analysis of the GITT solution for the temperature field, three lines across the IGBT module were selected, as illustrated by the red lines in Fig. 15a–c, along the x and z coordinates, respectively, indicating the positions where this convergence analysis is addressed.

Fig. 16a, b show the temperature profiles varying along the x and z coordinates, respectively, for different truncation orders (MT) in the temperature expansion, now with a larger source term $g = 10^9$ W/m3, more representative of the actual application [24]. In Fig. 16a, it is observed a graphical convergence of the temperature solution for truncation orders (MT) of 400 terms or higher, while in Fig. 16b, a higher truncation order, close to 1000 terms, is needed to warrant graphic convergence in the temperature expansion. The presence of the source term in a small region of the domain is responsible for the slower convergence in comparison to the previous test cases, a typical behavior

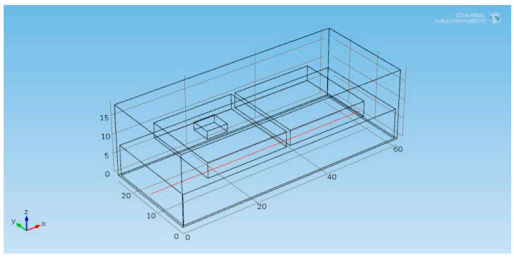

a. Red line indicating the positions along x for y = 12.5 mm, z = 2 mm, where temperature distributions are analyzed for the IGBT module (test case 3).

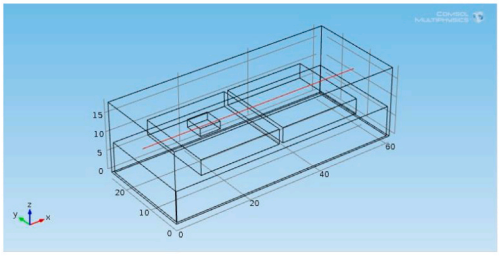

b. Red line indicating the positions along x for y = 12.5 mm, z = 13 mm, where temperature distributions are analyzed for the IGBT module (test case 3).

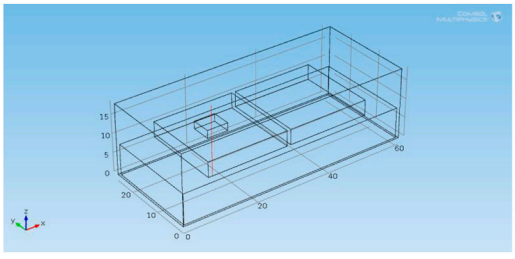

a-c. Red line indicating the positions along z for x=16.5 mm, y=12.5 mm, where temperature distributions are analyzed for the IGBT module (test case 3).

Fig. 15. (a) Red line indicating the positions along x for y = 12.5 mm, z = 2 mm, where temperature distributions are analyzed for the IGBT module (test case 3). (b) Red line indicating the positions along x for y = 12.5 mm, z = 13 mm, where temperature distributions are analyzed for the IGBT module (test case 3). a–c. Red line indicating the positions along z for x = 16.5 mm, y = 12.5 mm, where temperature distributions are analyzed for the IGBT module (test case 3). (For interpretation of the references to colour in this figure legend, the reader is referred to the web version of this article.)

in eigenfunction expansions, which suggests the use of a convergence acceleration technique, such as a filtering scheme or an integral balance approach, for convergence improvement [55]. Here, it has been chosen not to employ any sort of convergence acceleration technique so as to observe the applicability of the plain and direct GITT algorithm in such

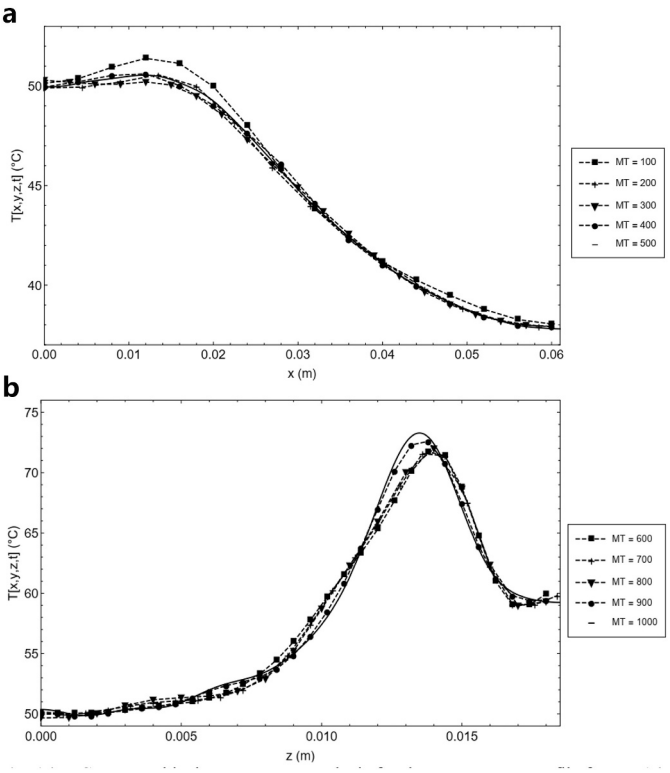

Fig. 16. (a) Convergence analysis of the temperature profile obtained by GITT for y = 12.5 mm, z = 2 mm and t = 20 s for the IGBT module (test case 3), with g = 10^9 W/m^3. (b) GITT graphical convergence analysis for the temperature profile for x = 16.5 mm, y = 12.5 mm and t = 20 s for the IGBT module (test case 3), with g = 10^9 W/m^3.

Table 12
Temperature convergence analysis via GITT along the x coordinate, for y = 12.5 mm, z = 13 mm, and t = 5 s for the IGBT module (test case 3).

	T(x,0.0125,0.013,5)						
M_T	0	0.01	0.02	0.03	0.04	0.05	0.06
100	30.77	37.03	39.80	30.24	26.83	26.05	25.56
200	31.03	36.93	43.05	29.55	26.93	25.71	24.99
300	30.88	35.82	43.17	30.06	27.26	26.10	25.49
400	31.43	35.63	44.31	30.00	27.33	26.23	25.35
500	31.46	35.30	45.40	29.63	27.63	26.00	25.48
600	31.41	35.42	44.98	29.81	27.19	26.09	25.65
700	31.38	35.54	45.07	29.84	27.20	26.09	25.55
800	31.36	35.59	45.35	29.82	27.22	26.08	25.56
900	31.42	35.60	45.61	29.83	27.04	26.31	25.58
1000	31.33	35.48	45.78	29.84	27.09	26.32	25.60
1100	31.31	35.49	45.80	29.79	27.10	26.32	25.59
Numerical (COMSOL) [56]	30.91	35.72	46.18	29.89	27.27	26.24	25.71
Deviation (%)	1.3	0.67	0.84	0.35	0.64	0.30	0.49

complex heterogeneous configurations, even without any convergence enhancement measure. Nevertheless, convergence of the eigenfunction expansion is still warranted at this critical region for the device thermal design as can be noticed to the graph scale in Fig. 16b.

Tables 12 and 13 illustrate the temperature convergence at different positions of the IGBT module along the x and z coordinates, respectively, with source term g = 10^9 W/m^3. It can be observed through Table 12 that at least three significant digits are converged at the positions evaluated along the x-coordinate, at y = 12.5 mm, z = 13 mm for time t = 5 s. For the positions shown in Table 13 along the z-coordinate, at x = 16.5 mm, y = 12.5 mm at time t = 5 s, practically three significant digits are converged. Also, the relative deviations with respect to the fully numerical solution (maximum size of the element

Table 13
Temperature convergence analysis via GITT along the z coordinate, for x = 16.5 mm, y = 12.5 mm, and t = 5 s for the IGBT module (test case 3).

	T(0.0165,0.0125,z,5)						
M_T	0	0.003	0.006	0.009	0.012	0.015	0.018
100	34.28	34.48	35.63	37.52	39.76	43.79	45.34
200	33.56	33.82	35.69	38.93	42.80	47.60	42.11
300	33.12	33.32	35.51	39.29	43.97	49.96	40.49
400	33.27	33.43	35.45	39.79	45.29	50.37	41.01
500	33.61	33.47	34.86	39.38	46.49	50.10	42.36
600	33.38	33.56	34.54	39.18	48.42	51.73	42.73
700	33.29	33.91	34.53	38.63	48.88	51.71	42.33
800	33.98	34.00	34.74	38.42	49.07	51.62	42.10
900	33.49	33.68	35.17	38.08	50.11	50.43	42.24
1000	33.69	33.66	35.26	38.19	50.37	50.01	42.11
1100	33.35	33.92	35.08	38.44	50.23	49.89	42.04
Numerical (COMSOL) [56]	33.21	33.57	34.84	38.29	49.41	49.12	41.53
Deviation (%)	0.42	1.02	0.69	0.39	1.66	1.57	1.21

equal to 6.10 mm) was below 1.3% for Table 12 and below 1.66% for Table 13, confirming the excellent agreement between the numerical and hybrid approaches.

Fig. 17a, b provide a comparison between the hybrid (GITT) and numerical (COMSOL) solutions, for temperature distributions along the x and z coordinates, respectively, according to the red lines in Fig. 15a, c. In both figures, the GITT solution was obtained with 1200 terms in the auxiliary eigenfunction expansion, with 500 and 1100 terms in the temperature expansion, respectively. The COMSOL simulation in both cases was obtained with a mesh element of a maximum size of 6.1 mm, with relative and absolute tolerances set to 10^{-3} and 10^{-4}, respectively. It can be seen from this comparison that the hybrid and numerical solutions are quite adherent to the graph scale, confirming the excellent agreement between them, previously illustrated in Tables 12 and 13. The only noticeable slight deviations between the two solutions are within the heat generation region, as observable from Fig. 17b.

5. Conclusions

Transient three-dimensional heat conduction in heterogeneous media was analyzed through the integral transform method (GITT), for three different situations characterized by both continuous but multi-scale or abrupt discontinuous variations of the diffusion equation space variable coefficients. First, the transient heat conduction problem in a FGM with thermophysical properties varying simultaneously in the x, y, and z directions was analyzed, followed by an example dealing with a composite media formed by a matrix filler material and with inclusions composed by spheres and cylinders of different thermophysical properties. Finally, an application dealing with a power electronics IGBT module with internal heat generation was considered. The single domain reformulation strategy was employed, when required by the presence of subregions, to rewrite the physical properties as space variable coefficients within one single diffusion equation for the whole domain. In the first test case, the solution obtained through GITT is critically compared with the numerical solution obtained through the NDSolve routine of the *Mathematica* platform, which implements the Method of Lines for partial differential equations. The second and third test cases were solved both through GITT and the COMSOL Multiphysics 4.4 simulation platform, which adopts the finite element method. Recent updates of the symbolic computation platform *Mathematica* have added interesting features that can be employed in more easily solving a wide range of convection-diffusion problems through hybrid numerical-analytical integral transforms. Among these new features, the integration over regions can be quite useful in dealing with heterogeneous media with different geometries of the sub-regions, as here demonstrated. For all test cases here implemented, an excellent agreement between the hybrid and numerical solution methodologies was achieved. While the general theoretical

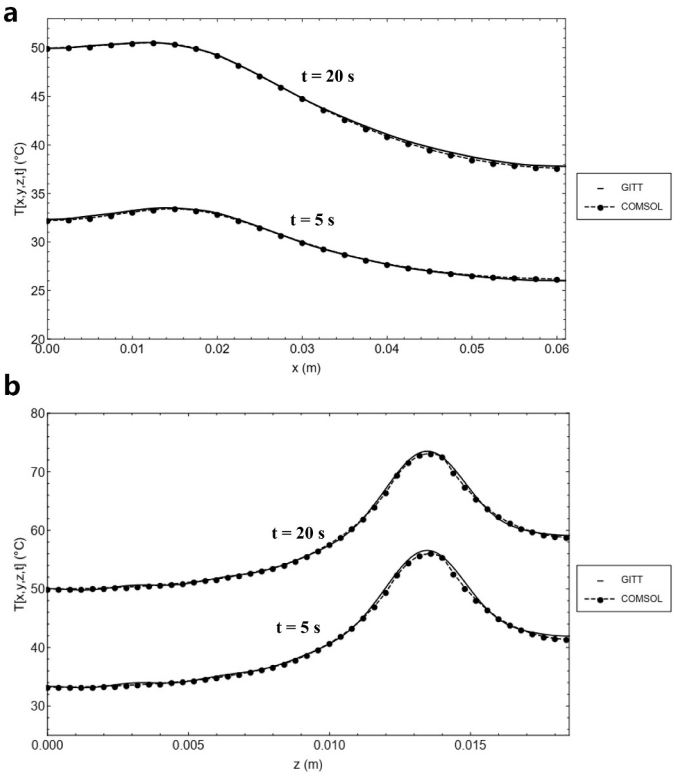

Fig. 17. (a) Comparison between the hybrid (GITT) and numerical (COMSOL) [56] solutions for the temperature distribution along the x-coordinate, for y = 12.5 mm, z = 2 mm at times t = 5 s and t = 20 s, for the IGBT module (test case 3), with g = 10^9 W/m^3. (b) Comparison between the hybrid (GITT) and numerical (COMSOL) [56] solutions for the temperature distribution along the z-coordinate, for x = 16.5 mm, y = 12.5 mm at times t = 5 s and t = 20 s, for the IGBT module (test case 3), with g = 10^9 W/m^3.

background of the present approach has already been established in previous works, a systematic demonstration of its use in transient three-dimensional heat conduction in heterogeneous media, for three different classes of medium heterogeneities, deserved a more detailed presentation in terms of computational algorithm and convergence demonstration. The present hybrid numerical-analytical approach is particularly advantageous in intensive computational tasks, when numerous evaluations of the original posed problem needs to be undertaken and accuracy is at a premium, such as in optimization, real time simulation, inverse problem analysis, and simulation under uncertainty.

Declaration of competing interest

The authors declare that they have no known competing financial interests or personal relationships that could have appeared to influence the work reported in this paper.

Acknowledgements

This work was partially supported by FAPERJ, CNPq and CAPES, all of them research sponsoring agencies in Brazil.

Contributions of individual authors

Anderson P. de Almeida – solution derivation, codes implementation, numerical analysis, and analysis of results.

Carolina P. Naveira-Cotta – selection of test cases, solution methodology development, analysis of results, manuscript preparation.

Renato M. Cotta - solution methodology development, numerical analysis, results interpretation, manuscript preparation.

References

[1] W.D. Callister Jr., D.G. Rethwisch, Materials Science and Engineering: An Introduction, 9th edition, Wiley, 2013.
[2] D.K. Jha, T. Kant, R.K. Singh, A critical review of recent research on functionally graded plates, Compos. Struct. 96 (2013) 833–849.
[3] I. Peralta, V.D. Fachinotti, J.C. Álvarez Hostos, A brief review on thermal metamaterials for cloaking and heat flux manipulation, Adv. Eng. Mater. 22 (2020) 1901034.
[4] S. Kakaç, H. Yüncü, K. Hijikata, Cooling of Electronic Systems, NATO ASI Series (NSSE), Vol. 258 Kluwer Academic Publishers, 1994.
[5] S.H. Lin, Transient conduction in heterogeneous media, Int. Commun. Heat Mass Transf. 10 (1992) 165–174.
[6] E. Divo, A. Kassab, Generalized boundary integral equation for transient heat conduction in heterogeneous media, J. Thermophys. Heat Transf. 12 (3) (1998) 364.
[7] O. Fudym, B. Ladevie, J.C. Batsale, A Seminumerical approach for heat diffusion in heterogenous media: one extension of the analytical Quadrupole method, Num. Heat Transf. B Fundam. 42 (2002) 325–348.
[8] A. Sutradhar, G.H. Paulino, L.J. Gray, Transient heat conduction in homogeneous and non-homogeneous materials by the Laplace transform Galerkin boundary element method, Eng. Anal. Bound. Elem. 26 (2002) 119–132.
[9] F. Danes, B. Garnier, T. Dupuis, Predicting, measuring and tailoring the transverse thermal conductivity of composites from polymer matrix and metal filler, Int. J. Thermophys. 24 (2003) 771–784.
[10] A. Sutradhar, G.H. Paulino, The simple boundary element method for transient heat conduction in functionally graded materials, Comput. Methods Appl. Mech. Eng. 193 (2004) 4511–4539.
[11] Y. Dai, W. Tan, Q. Sun, Y.D. Li, Effect of different thermal conductivity functions on temperature fields in FGM, J. Mater. Process. Technol. 187-188 (2007) 212–214.
[12] C.P. Naveira-Cotta, R.M. Cotta, H.R.B. Orlande, O. Fudym, Eigenfuction expansions for transient diffusion in heterogeneous media, Int. J. Heat Mass Transf. 52 (2009) 5029–5039.
[13] B. Du, J. Hudgins, E. Santi, A. Bryant, P. Palmer, H. Mantooth, Transient electro-thermal simulation of power semiconductor devices, IEEE Trans. Power Eletronics 25 (1) (2010) 237–248.
[14] C.P. Naveira-Cotta, R.M. Cotta, H.R.B. Orlande, Inverse analysis with integral transformed temperature fields for identification of thermophysical properties functions in heterogeneous media, Int. J. Heat Mass Transf. 54 (7–8) (2011) 1506–1519.
[15] D.C. Knupp, C.P. Naveira-Cotta, J.V.C. Ayres, H.R.B. Orlande, R.M. Cotta, Space-variable thermophysical properties identification in nanocomposites via integral transforms, Bayesian inference and infrared thermography, Inverse Probl. Sci. Eng. 20 (5) (2012) 609–637.
[16] D.C. Knupp, C.P. Naveira-Cotta, J.V.C. Ayres, R.M. Cotta, H.R.B. Orlande, Theoretical-experimental analysis of heat transfer in nonhomogeneous solids via improved lumped formulation, integral transforms and infrared thermography, Int. J. Thermal Sci. 62 (2012) 71–84.
[17] D.C. Knupp, C.P. Naveira-Cotta, H.R.B. Orlande, R.M. Cotta, Experimental identification of thermophysical properties in heterogeneous materials with integral transformation of temperature measurements from infrared thermography, Exp. Heat Transf. 26 (2013) 1–25.
[18] D.M. Perkowski, On axisymmetric heat conduction problem for FGM layer on

homogeneous substrate, Int. Commun. Heat Mass Transf. 57 (2014) 157–162.
[19] Y. Jarny, A. Matine, N. Boyard, G. Legrain, P. Cartraud, Transient heat conduction within periodic heterogeneous media: a space-time homogenization approach, Int. J. Therm. Sci. 92 (2015) 217–229.
[20] S. Chen, B. Yang, C. Zheng, A lattice Boltzmann model for heat transfer in heterogeneous media, Int. J. Heat Mass Transf. 102 (2016) 637–644.
[21] H. Rihab, N. Moudhaffar, B.N. Sassi, P. Patrick, Enthalpic lattice Boltzmann formulation for unsteady heat conduction in heterogeneous media, Int. J. Heat Mass Transf. 100 (2016) 728–736.
[22] F. Gori, S. Corasaniti, Heat conduction in two and three-phase media with solid spherical particles of same diameter, Int. J. Therm. Sci. 112 (2016) 460–469.
[23] W.L. Chen, H.M. Chou, Y.C. Yang, Inverse estimation of the unknown base heat flux in irregular fins made of functionally graded materials, Int. Commun. Heat Mass Transf. 87 (2017) 157–163.
[24] P.R. d'Egmont, C.P. Naveira-Cotta, R.F.S. Dias, C.P. Tostado, F.P. Duda, K. Chen, Experimental-Theoretical Thermal and Electrical Analyses of Insulated Gate Bipolar Transistors (IGBT) Power Module, ITHERM -Sixteenth Intersociety Conference on Thermal and Thermomechanical Phenomena in Electronic Systems, May 30 – June 2, 2017, Orlando, FL.
[25] K. Wei, C. Zhang, X. Gong, T. Kang, The IGBT losses analysis and calculation of inverter for two-seat electric aircraft application, the 8th international conference on applied energy – ICAE2016, Energy Procedia 105 (2017) 2623–2628.
[26] H.M. Ali, M.J. Ashraf, A. Giovannelli, M. Irfan, T.B. Irshad, H.M. Hamid, F. Hassan, A. Arshad, Thermal management of electronics: an experimental analysis of triangular, rectangular and circular pin-fin heat sinks for various PCMs, Int. J. Heat Mass Transf. 123 (2018) 272–284.
[27] R. Kulchytsky-Zhyhailo, S.J. Matysiak, D.M. Perkowski, On thermal analysis of periodic composite coatings for a homogeneous conductive layer, Int. Commun. Heat Mass Transf. 91 (2018) 210–215.
[28] A.P. Almeida, C.P. Naveira-Cotta, R.M. Cotta, Integral transforms for transient three-dimensional heat conduction in heterogeneous media with multiple geometries and materials, paper # IHTC16-24583, Proc. of the 16th International Heat Transfer Conference – IHTC16, Beijing, China, August 10th–15th, 2018, pp. 1859–1866.
[29] Z.J. Fu, Q. Xi, W Chen, AHD Cheng, A boundary-type meshless solver for transient heat conduction analysis of slender functionally graded materials with exponential variations, Comput. Math. Appl. 76 (2018) 760–773.
[30] A.A. Delouei, A. Emamian, S. Karimnejad, H. Sajjadi, A closed-form solution for axisymmetric conduction in a finite functionally graded cylinder, Int. Commun. Heat Mass Transf. 108 (2019) 104280.
[31] A. Loeb, C. Earls, Analysis of heterogeneous computing approaches to simulating heat transfer in heterogeneous material, J. Parallel Distrib. Comput. 133 (2019) 1–17.
[32] Q. Xi, Z.J. Fu, T. Rabczuk, An efficient boundary collocation scheme for transient thermal analysis in large-size-ration functionally graded materials under heat load source, Comput. Mech. 64 (2019) 1221–1235.
[33] W. Qu, C.M. Fan, Y. Zhang, Analysis of three-dimensional heat conduction in functionally graded materials by using a hybrid numerical method, Int. J. Heat Mass Transf. 145 (2019) 118771.
[34] A.A. Delouei, A. Emamian, S. Karimnejad, H. Sajjadi, D. Jing, Two-dimensional analytical solution for temperature distribution in FG hollow spheres: general thermal boundary conditions, Int. Commun. Heat Mass Transf. 113 (2020) 104531.
[35] R.M. Cotta, Hybrid numerical-analytical approach to nonlinear diffusion problems, Numer. Heat Transf. B 17 (1990) 217–226.
[36] R. Serfaty, R.M. Cotta, Integral transform solutions of diffusion problems with nonlinear equation coefficients, Int. Commun. Heat Mass Transf. 17 (6) (1990) 851–864.
[37] R.M. Cotta, Integral Transforms in Computational Heat and Fluid Flow, CRC Press, Boca Raton, FL, 1993.
[38] R.M. Cotta, M.D. Mikhailov, Heat Conduction: Lumped Analysis, Integral Transforms, Symbolic Computation, Wiley-Interscience, Chichester, UK, 1997.
[39] R.M. Cotta, D.C. Knupp, C.P. Naveira-Cotta, L.A. Sphaier, J.N.N. Quaresma, Unified integral transforms algorithm for solving multidimensional nonlinear convection-diffusion problems, Numer. Heat Transf. A 63 (2013) 840–866.
[40] R.M. Cotta, D.C. Knupp, C.P. Naveira-Cotta, Analytical heat and fluid flow in microchannels and microsystems, Mechanical Eng. Series, Springer-Verlag, 2016.
[41] R.M. Cotta, D.C. Knupp, J.N.N. Quaresma, Analytical methods in heat transfer, in: Francis A. Kulacki (Ed.), Handbook of Thermal Science and Engineering, Chapter 1, Springer International Publishing, 2017.
[42] R.M. Cotta, C.P. Naveira-Cotta, D.C. Knupp, J.L.Z. Zotin, P.C. Pontes, A.P. Almeida, Recent advances in computational-analytical integral transforms for convection-diffusion problems, Heat Mass Transf. 54 (2018) 2475–2496 Invited Paper.
[43] R.M. Cotta, D.C. Knupp, K.M. Lisboa, C.P. Naveira-Cotta, J.N.N. Quaresma, J.L.Z. Zotin, Integral transform benchmarks of diffusion, convection-diffusion, and conjugated problems in complex domains, in: A.K. Runchal (Ed.), 50 Years of CFD in Engineering Sciences –A Commemorative Volume in Memory of D. Brian Spalding, Springer-Verlag, 2020, pp. 719–750 Chapter 20.
[44] M.D. Mikhailov, R.M. Cotta, Integral transform method for eigenvalue problems, Commun. Numer. Methods Eng. 10 (1994) 827–835.
[45] L.A. Sphaier, R.M. Cotta, Integral transform analysis of multidimensional eigenvalue problems within irregular domains, Numer. Heat Transf. B Fundam. 38 (2000) 157–175.
[46] D.C. Knupp, C.P. Naveira-Cotta, R.M. Cotta, Theoretical analysis of conjugated heat transfer with a single domain formulation and integral transforms, Int. Commun. Heat Mass Transf. 39 (3) (2012) 355–362.
[47] D.C. Knupp, C.P. Naveira-Cotta, R.M. Cotta, Theoretical–experimental analysis of conjugated heat transfer in nanocomposite heat spreaders with multiple microchannels, Int. J. Heat Mass Transf. 74 (2014) 306–318.
[48] D.C. Knupp, R.M. Cotta, C.P. Naveira-Cotta, S. Kakaç, Transient conjugated heat transfer in microchannels: integral tranforms with single domain formulation, Int. J. Therm. Sci. 88 (2015) 248–257.
[49] D.C. Knupp, F.S. Mascouto, L.A.S. Abreu, C.P. Naveira-Cotta, R.M. Cotta, Conjugated heat transfer in circular microchannels with slip flow and axial diffusion effects, Int. Commun. Heat Mass Transf. 91 (2018) 225–233.
[50] D.C. Knupp, R.M. Cotta, C.P. Naveira-Cotta, Fluid flow and conjugated heat transfer in arbitrarily shaped channels via single domain formulation and integral transforms, Int. J. Heat Mass Transf. 82 (2015) 479–489.
[51] J.L.Z. Zotin, D.C. Knupp, R.M. Cotta, Conjugated heat transfer in complex channel-substrate configurations: hybrid solution with total integral transformation and single domain formulation, Proc. of ITherm 2017 – Sixteenth Intersociety Conference on Thermal and Thermomechanical Phenomena in Electronic Systems, Paper #435, Orlando, FL, USA, May 30th –June 2nd, 2017.
[52] R.M. Cotta, C.P. Naveira-Cotta, D.C. Knupp, Enhanced eigenfunction expansions in convection-diffusion problems with multiscale space variable coefficients, Numer. Heat Transf. A Appl. 70 (5) (2016) 492–512.
[53] S. Wolfram, Mathematica, Version 11.3, Wolfram Research Inc., Champaign, 2018.
[54] E.J. Correa, R.M. Cotta, H.R.B. Orlande, On the reduction of computational costs in eigenfunction expansions of multidimensional diffusion problems, Int. J. Numer. Meth. Heat Fluid Flow 7 (7) (1997) 675–695.
[55] A.R. Almeida, R.M. Cotta, A comparison of convergence acceleration schemes for eigenfunction expansions of partial differential equations, Int. J. Numer. Meth. Heat Fluid Flow 6 (6) (1996) 85–97.
[56] COMSOL Multiphysics: Multiphysics Modeling, Finite Element Analysis and Engineering Simulation Software. V. 4.2, (2013).